

UEOF: A Benchmark Dataset for Underwater Event-Based Optical Flow

Nick Truong*, Pritam P. Karmokar*, and William J. Beksi

The University of Texas at Arlington
Arlington, TX, USA

{nxt0706, pritam.karmokar}@mavs.uta.edu, william.beksi@uta.edu

Abstract

Underwater imaging is fundamentally challenging due to wavelength-dependent light attenuation, strong scattering from suspended particles, turbidity-induced blur, and non-uniform illumination. These effects impair standard cameras and make ground-truth motion nearly impossible to obtain. On the other hand, event cameras offer microsecond resolution and high dynamic range. Nonetheless, progress on investigating event cameras for underwater environments has been limited due to the lack of datasets that pair realistic underwater optics with accurate optical flow. To address this problem, we introduce the first synthetic underwater benchmark dataset for event-based optical flow derived from physically-based ray-traced RGBD sequences. Using a modern video-to-event pipeline applied to rendered underwater videos, we produce realistic event data streams with dense ground-truth flow, depth, and camera motion. Moreover, we benchmark state-of-the-art learning-based and model-based optical flow prediction methods to understand how underwater light transport affects event formation and motion estimation accuracy. Our dataset establishes a new baseline for future development and evaluation of underwater event-based perception algorithms. The source code and dataset for this project are publicly available at <https://robotic-vision-lab.github.io/ueof>.

1. Introduction

Unmanned underwater vehicles (UUVs) require reliable perception systems for tasks such as localization [11], mapping [22, 46, 57], navigation [1, 2, 45, 53], docking [9, 34, 59], examination [4, 43], inspection [32, 56], object pose estimation [42, 44], and manipulation [49, 61]. Nevertheless, underwater vision-based perception remains extremely challenging due to the complex light-medium interactions that cause rapid attenuation, wavelength-dependent color

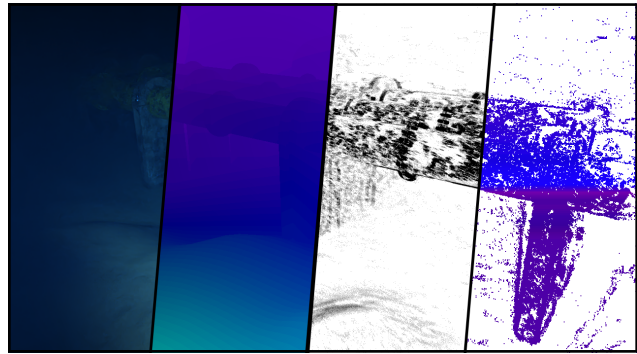


Figure 1. An illustration of data and ground-truth modalities from the UEOF dataset. Our dataset assembles physically-realistic underwater RGB imagery, ground-truth optical flow, camera egomotion, and temporally dense event streams, enabling the benchmarking of multimodal event-based optical flow estimation algorithms.

shifts, low contrast, and strong backscatter from suspended particles [3, 28, 55]. These effects degrade the performance of conventional cameras, especially during fast motion or in low-light, turbid, or high-dynamic range (HDR) conditions.

Compared to a frame-based camera, an event camera provides complementary advantages in challenging underwater scenarios. The asynchronous, high temporal resolution output of an event camera offers robustness to motion blur and HDR lighting, making it well-suited for visual odometry, optical flow estimation, and simultaneous localization and mapping (SLAM) in these environments. Yet, advancements in underwater event-based perception have been significantly constrained by a critical lack of data. Current underwater event-based datasets rarely include accurate ground truth for motion and optical flow since light detection and ranging and motion-capture systems do not function reliably underwater. As a result, algorithm development and benchmarking have relied predominantly on terrestrial datasets or synthetic data.

To bridge this gap, we introduce a new underwater event-based optical flow (UEOF) dataset generated by applying

* Indicates equal contribution.

high-quality video-to-event conversion to physically-based ray-traced (PBRT) RGBD sequences, Fig. 1. In particular, we obtain pseudo-event streams that capture the true temporal dynamics of the scene, while preserving accurate ground-truth optical flow and depth. This approach circumvents the limitations of both real-world data collection and rasterization-based simulators. It provides the first benchmark that combines physically accurate underwater rendering with temporally dense event data for motion estimation. We summarize our contributions as follows.

1. We present a synthetic underwater dataset that couples PBRT rendering with high temporal resolution pseudo-events through video-to-event conversion, enabling event-based evaluation under realistic underwater physics.
2. We provide dense ground-truth optical flow, depth, and pose from PBRT simulation, making this the first underwater dataset suitable for benchmarking event-based optical flow algorithms.
3. We benchmark a wide range of event-based optical flow techniques, including state-of-the-art event-driven and multimodal contrast maximization (CM) approaches, revealing the failure modes and domain-gap challenges unique to underwater scenes.
4. We analyze how underwater optical phenomena (*e.g.*, attenuation, backscatter, caustics, turbidity) affect event generation and event representations, offering insight into the suitability of event cameras for underwater perception.

Our dataset establishes a foundation to study event-based motion estimation in underwater environments and paves the way to realize robust multimodal perception systems for UUV autonomy.

The remainder of this paper is organized as follows. In Sec. 2, we review the landscape of existing underwater datasets and event simulators, identifying the critical gaps in ground truth availability that motivates our work. Sec. 3 details the proposed data generation pipeline, describing the integration of high-fidelity ray tracing with event simulation to produce the UEOF dataset. We present a comprehensive benchmarking of state-of-the-art supervised, unsupervised, and model-based algorithms along with a critical analysis of how underwater optical phenomena impacts estimation performance in Sec. 4. Finally, we conclude in Sec. 5 and discuss future directions for underwater event-based perception.

2. Related Work

2.1. Real-World Underwater Event Datasets

Several datasets contain real-world underwater event data, yet none capture ground-truth optical flow due to the difficulty of obtaining accurate motion supervision. For exam-

ple, DAVIS-NUIUIED [5] furnishes frame and event data recorded under non-uniform illumination to support underwater image enhancement research, without motion or pose estimations. FLSea [47] provides stereo RGB images and inertial measurement unit (IMU) data for underwater SLAM evaluation, sans optical flow or event annotations. The Aqua-Eye [35] dataset contains annotated DAVIS346 images, events, and fused event-frame representations for detecting transparent marine organisms. UTNet [18] extends Aqua-Eye by integrating ResNet50 [20] with sub-manifold sparse convolutions for improved segmentation of transparent underwater objects. Although both datasets include events, they do not provide depth or optical flow ground truth.

The AquaticVision [46] dataset provides synchronized stereo DAVIS346 events, grayscale frames, and IMU data at high frequency, along with 6-DoF motion-capture ground truth. The sequences cover clear water, HDR conditions, and varying turbidity. An analysis shows that event representations such as time surfaces perform well in clear water, but degrade significantly in turbid scenes, while event packet and voxel-grid representations offer improved robustness. The dataset is designed for visual SLAM and benchmarking, yet it lacks optical flow annotations. Evt-SlowTV [37] generates synthetic events from YouTube videos using video-to-event conversion, including underwater exploration footage, however it is not designed for optical flow or SLAM evaluations.

2.2. Synthetic Underwater Scenes

Rasterization-based simulators and PBRT engines differ drastically in their ability to model underwater light transport. For instance, Gazebo [26], UUV Simulator [39], and Stonefish [7, 17] rely on shader-based approximations. They cannot simulate volumetric scattering, spectral attenuation, or photon transport, leading to unrealistic underwater imagery that is unsuitable for photometrically sensitive tasks [31, 60]. MIMIR-UW [1] is built atop Unreal Engine [13] and AirSim [52]. It provides synthetic images, segmentation masks, and 6-DoF ground truth for SLAM and object inspection, but it does not include optical flow. Similarly, OysterSim [33] simulates oyster reef monitoring with underwater scattering and includes IMU, sonar, and camera pose data, yet it does not have event-based optical flow data.

Ray-traced renderers such as Blender Cycles [8] and Unreal Engine simulate photon transport, spectral absorption, and volumetric scattering. VAROS [62] yields ray-traced underwater RGB imagery with depth and surface normals. LOFUE [12] extends this by adding *ground-truth optical flow*, making it one of the most physically realistic underwater datasets with optical-flow labels. PHISWID [23] simulates underwater color degradation using absorption,

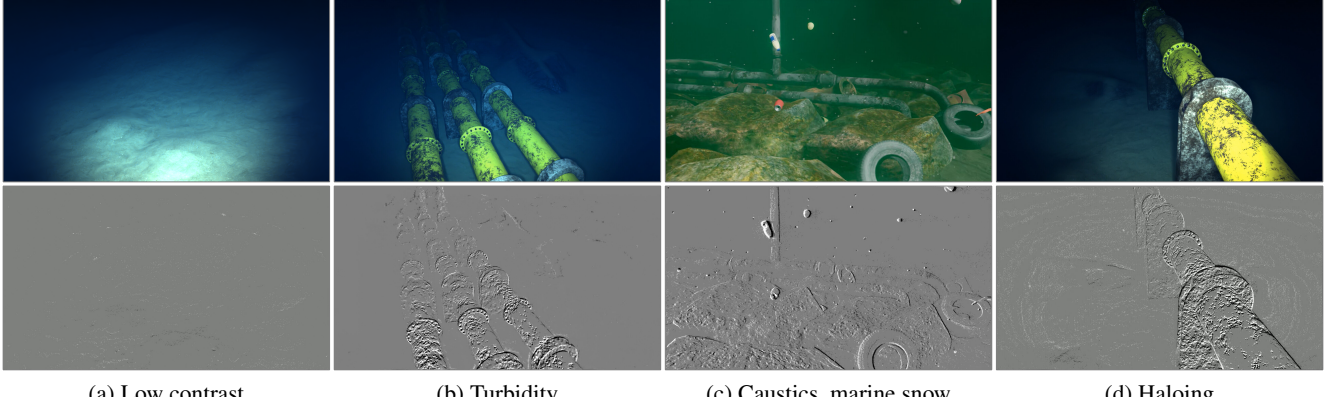


Figure 2. An illustration of key underwater visual degradation modes and their impact on event formation. RGB frames (top row) and the corresponding events (bottom row) are shown for a variety of challenging underwater scenarios.

scattering, and marine snow applied to terrestrial RGBD sequences. Although physically-based renderers produce highly realistic underwater imagery, they do not natively generate event data. This motivates the use of video-to-event conversion software such as the v2e [14, 21] toolbox.

2.3. Event Simulation

Existing simulators such as ESIM [48], MDR [36], and BlinkSim [30] rely on rasterized images and cannot model underwater light physics. eCARLA-scenes [40] adapts CARLA [10] for event data with a focus on autonomous driving. eStonefish-scenes [41] employs the Stonefish simulator to generate synthetic optical flow and events, but it inherits the limitations of rasterization (*i.e.*, no volumetric scattering and simplified light attenuation). Blender Cycles is utilized by EREBUS [27] for high-quality rendering. However, its event data is generated via the v2e toolbox and does not target optical flow. No existing event simulator models underwater light transport, no underwater event dataset provides ground-truth optical flow, and no ray-traced underwater dataset includes events, which beckons the need for new data generation pipelines. *To the best of our knowledge, UEOF is the first dataset to leverage PBRT RGBD data to generate temporally dense pseudo-events for evaluating event-based optical flow algorithms.*

3. Underwater Event-Based Optical Flow Dataset

3.1. Underwater Simulation

Realistic underwater rendering requires modeling complex interactions between light and a heterogeneous optical medium. Water contains dissolved organic matter, temperature gradients, salinity variations, air bubbles, suspended particles, and marine snow, all of which alter absorption and scattering in space and time. Consequently, underwater

image formation is nonlinear, wavelength-dependent, and strongly range-dependent, making it difficult to faithfully simulate. Underwater light transport involves wavelength-dependent attenuation, and both forward and back scattering governed by complex phase functions [3]. Accurate simulation requires solving the radiative transfer equation, typically via Monte Carlo photon simulation, which is computationally expensive and sensitive to optical parameters [51].

As highlighted in Fig. 2, optical properties vary with depth, water type (coastal vs. oceanic), turbidity, and environmental conditions [50]. Bubbles, turbulence, flickering caustics, and marine snow introduce temporal inconsistencies that are difficult to capture using static rendering pipelines [58]. Natural light attenuates rapidly with depth, producing low-light blue-green-shifted imagery [38]. Artificial illumination introduces strong backscatter, halos, and veiling glare whose appearance depends on the geometry of the light sources and the particle field [23]. Wavelength-dependent attenuation causes color shifts and contrast loss that cannot be captured by simple haze-style degradation models [28]. For many underwater scenes, the true reflectance or “water-free” reference appearance is unknown, complicating the validation of synthetic renderings [62].

Real-world underwater event datasets with dense ground-truth optical flow are nonexistent. Moreover, they rarely include accurate optical measurements, geometry, or lighting conditions. This makes it difficult to parameterize simulators and leads to significant domain gaps between synthetic and real imagery [29]. Furthermore, existing synthetic event simulators are built on rasterization pipelines that do not model volumetric light transport or scattering, limiting their applicability in the underwater domain. These fundamental challenges limit the fidelity of underwater rendering engines, an issue that becomes even more restrictive when simulating event data or generating training la-

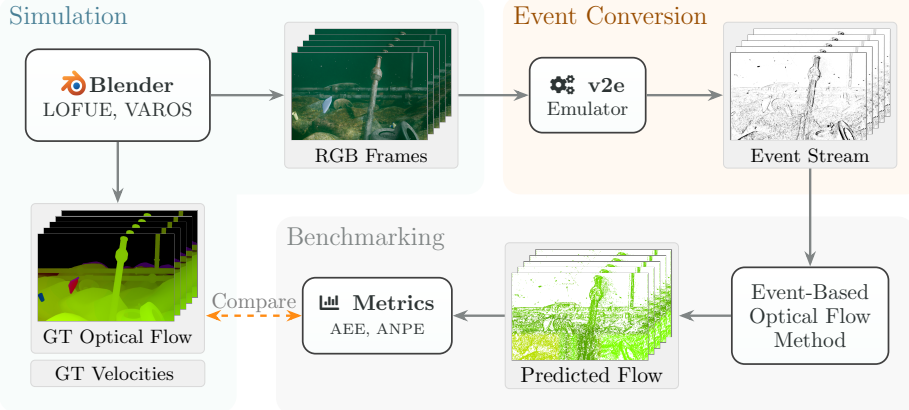


Figure 3. The UEOF data generation pipeline. First, Blender is utilized to render high-fidelity RGB frames and extract ground-truth data from the LOFUE and VAROS datasets. Next, the RGB frames undergo event conversion via the v2e toolbox. Finally, the resulting event streams are processed by event-based optical flow methods and the predicted flow is evaluated against the ground-truth data using standard endpoint error metrics.

belts such as optical flow. We address these issues via a high-fidelity pseudo-event dataset. Concretely, the UEOF dataset provides the following: (i) photometrically realistic RGB imagery rendered using Blender Cycles, (ii) asynchronous event streams emulated with the v2e toolbox, (iii) dense per-pixel optical flow ground truth, and (iv) camera velocities.

3.2. Simulation Sources

UEOF was built from two underwater ray-traced datasets that complement one another in scene complexity, motion patterns, and rendering realism. The first dataset, VAROS, simulates UUV operations across infrastructure inspection and seafloor exploration scenarios. We divide the VAROS data into five distinct scenes where each one contains the following: (i) lossless RGB images, (ii) surface normal vector images, (iii) metric depth maps, (iv) accurate 6-DoF ground-truth poses, (v) synchronized IMU data, and (vi) depth-gauge data. The scenes comprise pipes, man-made structures, and the natural seabed with physically correct illumination and scattering. Although optical flow is not provided, all dynamic motion arises purely from camera egomotion (*i.e.*, no independently moving objects), enabling perfect geometric reconstruction.

The second dataset, LOFUE, features complex underwater scenes with dynamic objects (*e.g.*, fish, vegetation, floating debris, *etc.*), varied water turbidity, and both static and moving cameras. Specifically, `scene1` and `scene5` feature a static camera, while `scene2`, `scene3`, and `scene4` present a moving camera simulating realistic vehicle motion. All imagery is rendered using Blender Cycles with physically-based light propagation, including volumetric scattering and spectral attenuation. LOFUE provides RGB frames and dense optical flow ground truth using the

add-on VisionBlender [6]. Together VAROS and LOFUE offer complementary strengths. LOFUE includes dynamic-object flow, while VAROS yields precise geometric and inertial measurements. Both datasets supply physically-grounded underwater imagery.

3.3. Event Data Generation

We generated asynchronous event streams from the rendered RGB sequences using the v2e toolbox, which models the behavior of a dynamic vision sensor (DVS). Standard v2e parameters are designed for terrestrial scenes and require adaptation for underwater imagery, where contrast is heavily degraded due to scattering and spectral attenuation. For each source sequence, the raw frames were first converted to video at 30 FPS and 10 FPS from the LOFUE and VAROS datasets, respectively. Then, the v2e software was used to perform slow-motion interpolation such that no pixel translates more than 1 px between adjacent frames, ensuring realistic event triggering under fast camera motion or low-light visibility.

To increase DVS sensitivity in low-texture or heavily attenuated regions (*e.g.*, sandy seafloors), we lowered the positive/negative thresholds from the default values. This improves the event density in regions that would otherwise fail to produce measurable illumination changes. Nonetheless, lower thresholds, θ_{nominal} , risk false triggering in darker areas. We countered this by reducing the threshold variation, σ_θ , effectively suppressing fixed-pattern noise without blurring genuine edges. Events are exported via the HDF5 file structure as a sequence of (t, x, y, p) tuples, where t is the timestamp, (x, y) is the pixel location, and p is the polarity of the fired event. An overview of the UEOF data generation pipeline is shown in Fig. 3.

3.4. Ground-Truth Data Generation

The UEOF dataset contains dense per-pixel optical flow maps and 6-DoF camera velocity ground truth for all sequences. The ground-truth optical flow is stored in the standard Middlebury format (`.flo`), aligned with each RGB frame. For the LOFUE sequences, we utilized the precomputed optical flow ground truth provided by the authors. The VAROS sequences do not provide optical flow data. Therefore, we reconstructed dense optical flow via geometric back-projection. Specifically, valid pixels \mathbf{u}_t were back-projected into 3D points $\mathbf{P}_t = \pi^{-1}(\mathbf{u}_t, D_t(\mathbf{u}_t))$ using the provided metric depth map D_t and intrinsic parameters. These points were then transformed to the subsequent frame via the rigid-body motion $\mathbf{T}_{t \rightarrow t+1} \in SE(3)$ yielding the induced flow $\Delta \mathbf{u} = \pi(\mathbf{T}_{t \rightarrow t+1} \mathbf{P}_t) - \mathbf{u}_t$. We also applied a geometric occlusion check by comparing transformed points projected onto the target image plane, and their computed depth z_{t+1} against the target depth map D_{t+1} . Correspondences were considered valid only if they fell within image bounds, satisfied the near-plane constraint ($z_{t+1} > 0.1$ m), and passed the visibility test ($z_{t+1} \leq D_{t+1} + \epsilon$). We set the tolerance $\epsilon = 0.01$ m. This filters out occluded regions where the projected point lies behind the visible surface.

The 6-DoF linear (\mathbf{v}) and angular ($\boldsymbol{\omega}$) ground-truth camera ego-velocities are provided for all the sequences in the UEOF dataset. These measurements are stored and compressed as `.npz` archives containing three primary keys: `lin_vel`, `ang_vel`, and `timestamps` in microseconds. For the LOFUE sequences, we utilized the Blender Python API to directly extract the camera's instantaneous rigid-body velocity vectors in the camera coordinate frame at each render step (30 Hz). For the VAROS sequences, we derived the velocities from the provided high-frequency (200 Hz) ground-truth camera poses. Then, we computed the body-frame velocities using central finite differences on the position and quaternion parameters by converting quaternion derivatives to angular velocity via the standard kinematic relationship $\boldsymbol{\omega} = 2\hat{\mathbf{q}}^{-1} \otimes \dot{\mathbf{q}}$, where \otimes denotes the Hamilton product, $\hat{\mathbf{q}}$ is the unit quaternion representing camera orientation, and $\dot{\mathbf{q}}$ is its time derivative.

3.5. Dataset Statistics

Using the proposed simulation pipeline, we generated 12 minutes and 51 seconds of data across 13,714 RGB frames. This results in a total of 4.94 billion events across all scenes. In summary, the UEOF dataset exhibits the following key characteristics.

- **High Resolution:** As indicated in Tab. 1, the dataset provides event streams in two spatial resolutions: 960×540 and 1280×720 . Notably, the 1280×720 resolution coincides with the sensor specifications of the Prophesee EVK4 HD with the Sony IMX636ES HD sensor, a

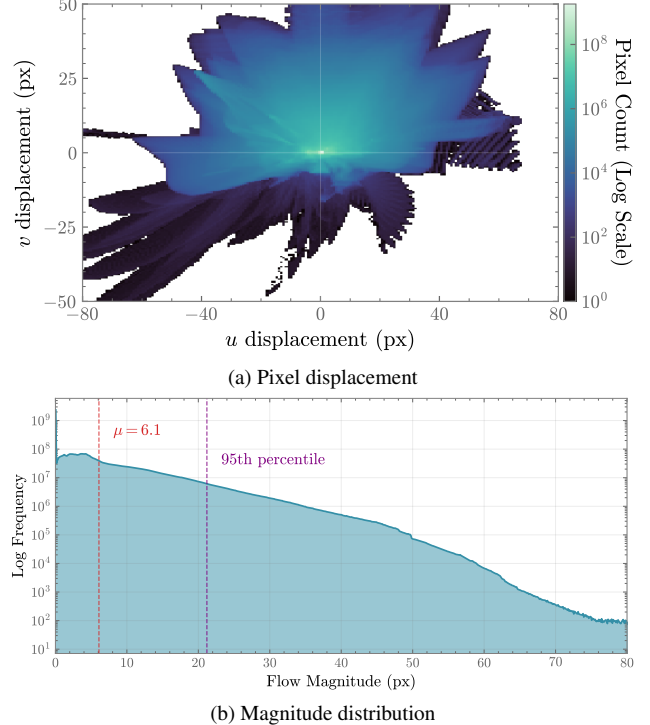


Figure 4. Optical flow statistics for the UEOF dataset: (a) the joint distribution of (u, v) pixel displacements highlight dense coverage of motion directions; (b) the semi-log histogram shows a heavy-tailed distribution with a mean of 6.1 px.

widely used event camera. This alignment minimizes the simulation-to-reality gap and establishes a realistic benchmark for evaluating event-based optical flow estimation methods at standard sensor resolutions.

- **Temporally Dense:** The LOFUE scenes operate at 30 FPS for RGB frames, with synchronized ground-truth velocities and optical flow evaluation provided at 30 Hz. The VAROS scenes run at 10 FPS for RGB frames (evaluations at 10 Hz). However, the camera ego-velocities are derived from high-precision logs recorded at 200 Hz. In total, the dataset provides 13,704 evaluation intervals.
- **Comprehensive Motion:** As displayed in Fig. 4, the dataset exhibits a high dynamic range of motion, with a mean flow magnitude of 6.1 px and a median of 3.6 px. The motion distribution is heavy-tailed. While a majority of pixels undergo moderate displacement (with a 95th percentile of 21.20 px), the dataset also includes significant high-magnitude flow upwards of 80 px.

4. Evaluation

4.1. Experimental Setup

We conducted experiments on all scenes of the UEOF dataset. The event-based optical flow metrics include the

| Dataset | Sensor / Sim. | Res ($W \times H$) | Duration | Modalities | | Ground Truth | |
|---|----------------------------|--------------------------------------|---------------|------------|--------|--------------|-----|
| | | | | RGB | Events | Flow | Vel |
| <i>Real-World Datasets</i> | | | | | | | |
| AquaticVision [46] | DAVIS346 | 346 \times 260 | 13m06s | - | ✓ | - | ✓ |
| OsloMet [49] | DAVIS346 | 346 \times 260 | - | - | ✓ | - | ✓ |
| Aqua-eye [35] | DAVIS346 | 346 \times 260 | - | ✓ | ✓ | - | - |
| DAVIS-NUUIUED [5] | DAVIS346 | 346 \times 260 | - | ✓ | ✓ | - | - |
| <i>Synthetic and Converted Datasets</i> | | | | | | | |
| EvtSlowTV [37] | YouTube \rightarrow ESIM | Var. | 9000m | ✓ | ✓ | - | - |
| eStonefish [41] | Stonefish | 1280 \times 720 | 6m | - | ✓ | ✓ | - |
| EREBUS [27] | Blender \rightarrow V2E | 1920 \times 1080 | - | ✓ | ✓ | - | - |
| UEOF (Ours) | Blender \rightarrow V2E | 1280 \times 720* | 12m51s | ✓ | ✓ | ✓ | ✓ |

Table 1. A comparison of underwater event-based datasets. While several datasets exist, UEOF is the first to provide ground-truth optical flow and camera ego-velocity derived from PBRT simulation. *Res*: resolution. *Flow*: optical flow. *Vel*: camera ego-velocity. ‘-’: duration not reported or available. *Includes subsets at 960 \times 540 resolution.

| Methods | scene1 | scene2 | scene3 | scene4 | scene5 |
|----------------------|----------------------|----------------------|----------------------|----------------------|----------------------|
| | AEE (\downarrow) |
| LB | | | | | |
| E-RAFT [16] | 8.67 | 9.05 | 10.52 | 8.64 | 16.32 |
| MotionPriorCMax [19] | 2.61 | <u>1.54</u> | 1.92 | 1.49 | <u>2.36</u> |
| MB | | | | | |
| EINCM [25] | <u>4.52</u> | 2.36 | <u>2.06</u> | 1.01 | 4.12 |
| MultiCM [54] | 5.10 | 1.37 | 2.42 | <u>1.37</u> | 2.27 |
| OPCM [24] | - | 1.62 | 2.14 | 1.93 | - |

Table 2. The average endpoint error (AEE) in pixels on the UEOF dataset (shallow-water environment) across five scenes ($dt = 1$). **Bold** indicates best, underline indicates second-best.

| Methods | scene1 | scene2 | scene3 | scene4 | scene5 |
|----------------------|----------------------|----------------------|----------------------|----------------------|----------------------|
| | AEE (\downarrow) |
| LB | | | | | |
| E-RAFT [16] | 5.82 | 10.11 | 4.88 | 7.64 | 3.61 |
| MotionPriorCMax [19] | 6.93 | <u>5.61</u> | 6.24 | 7.39 | 5.25 |
| MB | | | | | |
| EINCM [25] | 3.94 | <u>2.58</u> | <u>3.37</u> | <u>2.36</u> | <u>2.56</u> |
| MultiCM [54] | <u>4.44</u> | 2.39 | 3.32 | 2.05 | 2.35 |

Table 3. The average end-point error (AEE) in pixels on the UEOF dataset (deep-water environment) across five scenes at $dt = 1$. **Bold** indicates best, underline indicates second-best.

average endpoint error (AEE) as well as ANPE, which represents the percentage of pixels with an endpoint error lower than N pixels for $N \in \{1, 2, 3, 5, 10, 20\}$. To ensure a comprehensive evaluation, we benchmarked the UEOF dataset against representative state-of-the-art approaches categorized into two primary paradigms: learning-based (LB) and model-based (MB) algorithms. The LB techniques consist of supervised and unsupervised learning. Supervised techniques, like E-RAFT [16], leverage high-quality ground truth for training. Conversely, unsupervised learning algorithms, such as MotionPriorCMax [19], circumvent this by relying exclusively on the raw event data itself. Conversely, the MB methods stray away from neural networks and instead adopt traditional nonlinear optimization with contrast

maximization objectives.

To make the UEOF dataset more impactful, we first extended the existing dataloaders of each evaluated technique. This involved adapting the algorithm’s input to correctly handle our specified data formats. In the evaluations of the LB approaches, we utilized the checkpoints provided by each publication, which were pretrained on the DSEC [15] dataset. The MB methods used identical accumulated event window sizes for each respective scene. Otherwise, we maintained the default configurations and parameters. The configuration files and modified source code used for the evaluation are available on our project website.

4.2. Results

The quantitative results for shallow-water and deep-water environments are presented in Tabs. 2 and 4 and Tabs. 3 and 5, respectively. We note that the MB approaches MultiCM [54] and EINCM [25] achieved the lowest error rates, with EINCM [25] reaching a minimum AEE of 1.01 px in scene4 (shallow-water). Conversely, the LB model E-RAFT [16] exhibited the highest errors, peaking at 16.32 px in scene5 (shallow-water). In the deep-water environment, we observed a universal increase in error magnitudes across all techniques.

4.3. Analysis

Our experiments reveal a significant performance degradation for state-of-the-art event-based optical flow methods. Specifically, the results indicate that the limitations are a compounding interaction wherein underwater phenomena expose and heighten flaws in current event-based processing algorithms. Supervised approaches such as E-RAFT [16] exhibited high error rates when relying on pre-trained weights from the DSEC dataset. We hypothesize that this is due to the fact that the terrestrial datasets are dominated by high-frequency rigid edges (*e.g.*, buildings,

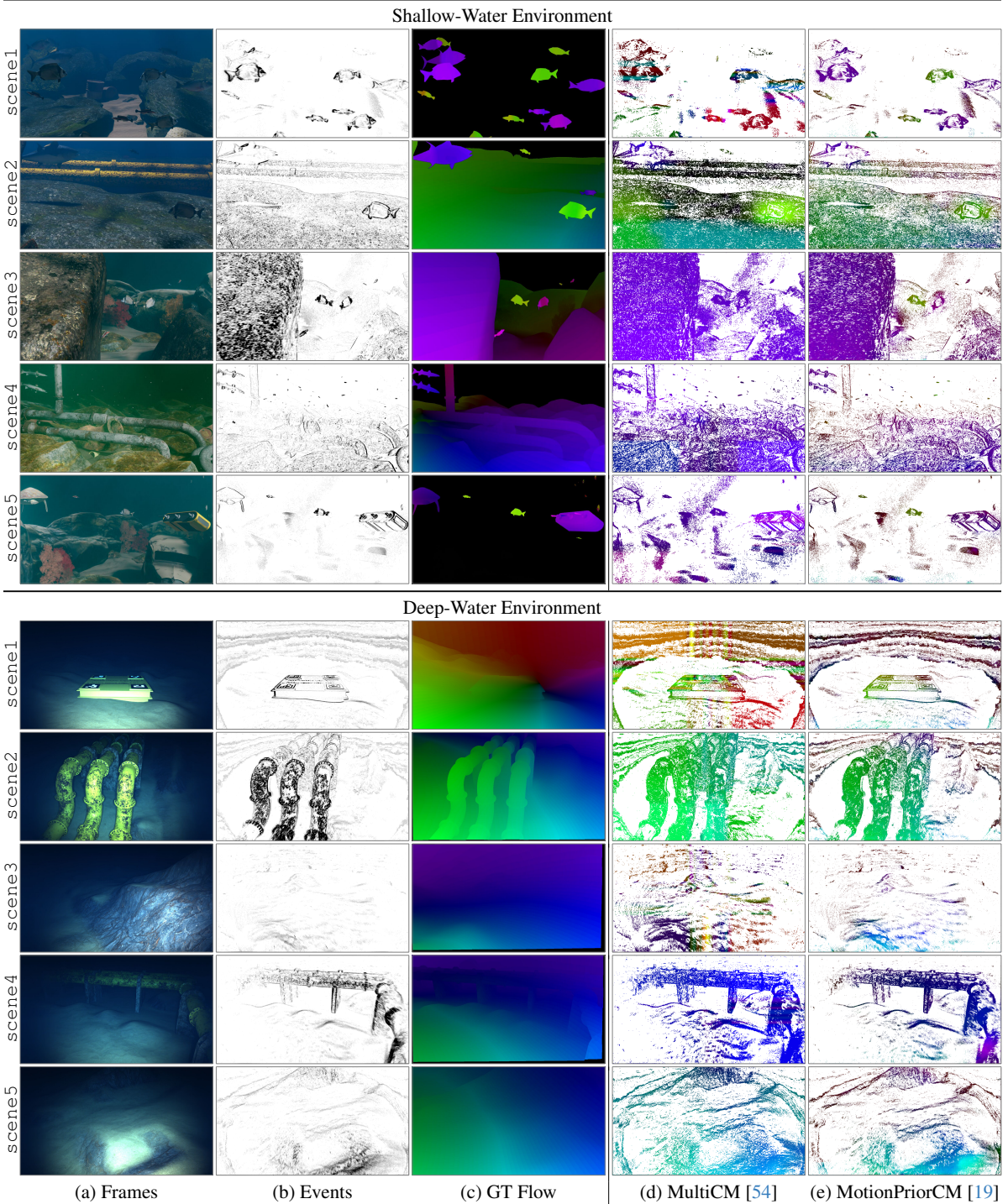


Figure 5. Qualitative event-based optical flow estimation results using the UEOF dataset. Columns (a-e) show the frames, events, ground-truth (GT) optical flow, and the predicted event-based optical flow using a representative MB (MultiCM [54]) and LB (MotionPriorCM [19]) method. The top five and bottom five rows correspond to the shallow-water and deep-water environment sequences, respectively. The optical flow direction and magnitude are encoded according to the color legend shown below.



| Methods | scene1 | | | | | | scene2 | | | | | | scene3 | | | |
|---------|----------------------|--------------|--------------|--------------|--------------|-------------|------------------|--------------|--------------|--------------|--------------|-------------|------------------|--------------|--------------|--------------|
| | A1PE (↓) | A2PE (↓) | A3PE (↓) | A5PE (↓) | A10PE (↓) | A20PE (↓) | A1PE (↓) | A2PE (↓) | A3PE (↓) | A5PE (↓) | A10PE (↓) | A20PE (↓) | A1PE (↓) | A2PE (↓) | A3PE (↓) | |
| LB | E-RAFT [16] | 59.24 | 47.72 | 42.30 | 36.10 | 26.52 | 9.43 | 97.9 | 92.70 | 85.10 | 66.80 | 23.50 | 4.00 | 90.64 | 72.78 | 57.19 |
| | MotionPriorCMax [19] | 83.13 | 30.53 | 21.38 | 12.62 | 3.61 | 1.20 | 56.16 | <u>18.28</u> | <u>8.10</u> | <u>3.25</u> | <u>1.06</u> | <u>0.17</u> | 72.10 | <u>24.20</u> | 11.53 |
| | EINCM [25] | 69.50 | 63.22 | 59.93 | 50.28 | 5.57 | <u>0.01</u> | 44.34 | 26.67 | 20.40 | 13.66 | 8.42 | 7.01 | 27.41 | 18.74 | <u>14.88</u> |
| | MultiCM [54] | 75.11 | 73.59 | 71.19 | 61.17 | <u>5.54</u> | <u>< 0.01</u> | 41.96 | 12.66 | 6.91 | 3.97 | 1.33 | 0.31 | <u>59.56</u> | 35.00 | 23.31 |
| MB | OPCM [24] | — | — | — | — | — | — | 58.47 | 25.14 | 11.17 | <u>3.33</u> | <u>0.60</u> | <u>< 0.01</u> | 72.80 | 33.45 | 19.66 |
| | scene4 | | | | | | scene5 | | | | | | scene3 (contd.) | | | |
| | E-RAFT [16] | 96.26 | 91.34 | 85.62 | 68.21 | 19.78 | 4.16 | 43.85 | <u>36.71</u> | 33.70 | 29.71 | 23.52 | 20.07 | 42.11 | 20.20 | 10.23 |
| | MotionPriorCMax [19] | 65.52 | <u>15.67</u> | 5.13 | <u>2.25</u> | <u>0.37</u> | 0.02 | 83.09 | 20.60 | 13.76 | 0.98 | <u>0.35</u> | <u>0.24</u> | 5.19 | <u>1.47</u> | <u>0.25</u> |
| MB | EINCM [25] | 18.88 | 8.92 | <u>6.22</u> | 3.79 | 1.10 | 0.30 | 75.61 | 66.22 | 58.84 | 35.92 | 4.11 | 0.88 | 10.60 | 6.20 | 1.60 |
| | MultiCM [54] | <u>41.39</u> | 18.27 | 9.23 | 3.80 | 0.58 | 0.20 | <u>69.33</u> | 40.26 | <u>23.54</u> | <u>10.00</u> | <u>1.50</u> | 0.08 | 12.52 | 3.42 | 0.54 |
| | OPCM [24] | 80.46 | 37.45 | 12.75 | <u>2.41</u> | 0.25 | <u>0.05</u> | — | — | — | — | — | — | <u>8.29</u> | <u>1.17</u> | 0.05 |

Table 4. The N-pixel error rates on the UEOF dataset (shallow-water environment) across five scenes at $dt = 1$. **Bold** indicates best, underline indicates second-best.

| Methods | scene1 | | | | | | scene2 | | | | | | scene3 | | | |
|---------|----------------------|--------------|--------------|--------------|--------------|--------------|-------------|--------------|--------------|--------------|--------------|-------------|-----------------|--------------|--------------|--------------|
| | A1PE (↓) | A2PE (↓) | A3PE (↓) | A5PE (↓) | A10PE (↓) | A20PE (↓) | A1PE (↓) | A2PE (↓) | A3PE (↓) | A5PE (↓) | A10PE (↓) | A20PE (↓) | A1PE (↓) | A2PE (↓) | A3PE (↓) | |
| LB | E-RAFT [16] | 72.43 | 51.13 | 38.96 | 23.72 | 8.63 | <u>4.13</u> | 98.37 | 94.41 | 89.66 | 77.83 | 42.58 | 5.92 | 59.61 | 41.97 | 31.88 |
| | MotionPriorCMax [19] | 92.70 | 81.71 | 69.04 | 47.35 | 21.45 | 5.65 | 84.83 | 70.28 | 59.20 | 42.94 | 16.66 | 2.20 | 85.97 | 70.72 | 59.64 |
| | EINCM [25] | 60.92 | 47.67 | 38.76 | 25.58 | 10.44 | 2.95 | 41.39 | 30.39 | 24.40 | 16.72 | 6.75 | 1.07 | 50.15 | 37.40 | 30.55 |
| | MultiCM [54] | 60.38 | 44.94 | 36.86 | 27.62 | 13.81 | 4.34 | <u>47.33</u> | <u>33.10</u> | <u>24.67</u> | <u>14.48</u> | <u>4.52</u> | 0.60 | 48.66 | 36.03 | 29.19 |
| MB | scene4 | | | | | | scene5 | | | | | | scene3 (contd.) | | | |
| | E-RAFT [16] | 69.48 | 53.99 | 47.92 | 40.25 | 16.08 | 4.06 | 65.11 | <u>45.71</u> | 33.23 | 20.13 | 7.09 | 1.34 | 19.44 | 7.96 | <u>3.13</u> |
| | MotionPriorCMax [19] | 87.87 | 78.54 | 72.07 | 60.35 | 26.36 | 3.35 | 85.94 | 71.70 | 59.70 | 37.66 | 13.29 | 2.11 | 42.71 | 18.86 | 4.94 |
| | EINCM [25] | 37.46 | 26.61 | 20.38 | 12.54 | 4.97 | <u>1.57</u> | 47.20 | <u>31.50</u> | <u>23.80</u> | <u>15.90</u> | <u>6.45</u> | <u>0.95</u> | 23.10 | 12.85 | 3.25 |
| | MultiCM [54] | <u>39.79</u> | 25.98 | 18.83 | 11.68 | 4.88 | <u>0.54</u> | 45.87 | 30.02 | 22.44 | 14.06 | 5.28 | 0.51 | <u>21.29</u> | <u>10.73</u> | 2.12 |

Table 5. The N-pixel error rates on the UEOF dataset (deep-water environment) across five scenes at $dt = 1$. **Bold** indicates best, underline indicates second-best.

vehicles, *etc.*). Conversely, underwater scenes, particularly in turbid waters, are defined by soft, low-frequency textures due to volumetric scattering. As a result, the supervised networks suffered from severe feature distribution shifts.

We also noticed that refractive caustics created high-contrast light patterns that traversed the seafloor independent of physical geometry. Consequently, contrast maximization approaches that rely on a brightness constancy assumption revealed a limitation in estimating optical flow from events that are not caused by motion. Since caustics generate dense, high-frequency event streams, we observed that this can cause CM objectives to falsely align and produce incorrect motion estimates. As shown in Fig. 5 (shallow-water scenes 1, 2, 3, and 5), a performance gap appears in dynamic sequences where independent objects (*e.g.*, fish) traverse in different directions. Methods such as MultiCM [54] failed to resolve these conflicting motions, while MotionPriorCMax [19] maintained robustness.

In addition, the error rates across all models evaluated on the deep-water environment are notably higher when compared to the shallow-water environment. We attribute this to the many adverse effects of the deep-water scenes, such as haloing from UUV lighting, poor contrast due to attenuation, and a low-texture seafloor. In comparison, the shallow-water scenes contain strong and consistent sunlight, which can create textures on the seabed. This provides more, albeit noisy, features for tracking. Finally, the evaluation re-

sults demonstrate that multimodal approaches, specifically those integrating velocity data like OPCM [24], vary in improvement on dynamic scenes over their non-multimodal counterparts.

5. Conclusion and Future Work

In this paper, we introduced UEOF, the first synthetic underwater dataset to leverage PBRT simulation with temporally dense event streams, accurate ground-truth optical flow, and ego-velocities. Our comprehensive benchmarking results reveal that state-of-the-art approaches, whether LB or MB, struggle to generalize from the terrestrial to the underwater domain. Thus, the UEOF dataset establishes a necessary baseline for advanced research, fostering the development of robust algorithms capable of handling the large domain gaps present in underwater environments. We anticipate that this benchmark dataset will accelerate progress towards reliable multimodal event-based perception for the next generation of UUVs. Our future work includes extending the UEOF dataset with additional data and ground-truth modalities, richer environmental diversity, and physically-grounded event noise models.

Acknowledgments

This material is based upon work supported by the Office of Naval Research under award number N000142512349.

References

[1] Olaya Álvarez-Tuñón, Hemanth Kanner, Luiza Ribeiro Mar- net, Huy Xuan Pham, Jonas le Fevre Sejersen, Yury Brod- skiy, and Erdal Kayacan. Mimir-uw: A multipurpose syn- thetic dataset for underwater navigation and inspection. In *Proceedings of the IEEE/RSJ International Conference on Intelligent Robots and Systems*, pages 6141–6148, 2023. 1, 2

[2] Abdelhakim Amer, Olaya Álvarez-Tuñón, Halil İbrahim Uğurlu, Jonas Le Fevre Sejersen, Yury Brodskiy, and Erdal Kayacan. Unav-sim: A visually realistic underwater robotics simulator and synthetic data-generation framework. In *Proceedings of the International Conference on Advanced Robotics*, pages 570–576. IEEE, 2023. 1

[3] Lucas Amparo Barbosa and Antonio Lopes Apolinario Jr. From physically based to generative models: A survey on underwater image synthesis techniques. *Journal of Imaging*, 11(5):161, 2025. 1, 3

[4] J Betancourt, W Coral, and J Colorado. An integrated rov solution for underwater net-cage inspection in fish farms using computer vision. *SN Applied Sciences*, 2(12):1946, 2020. 1

[5] Xiuwen Bi, Pengfei Wang, Tao Wu, Fusheng Zha, and Peng Xu. Non-uniform illumination underwater image enhancement via events and frame fusion. *Applied Optics*, 61(29): 8826–8832, 2022. 2, 6

[6] João Cartucho, Samyakh Tukra, Yunpeng Li, Daniel S. El- son, and Stamatia Giannarou. Visionblender: a tool to effi- ciently generate computer vision datasets for robotic surgery. *Computer Methods in Biomechanics and Biomedical Engineering: Imaging & Visualization*, 9(4):331–338, 2021. 4

[7] Patryk Cieślak. Stonefish: An advanced open-source sim- ulation tool designed for marine robotics, with a ros interface. In *Proceedings of OCEANS*, pages 1–6. IEEE, 2019. 2

[8] Blender Online Community. Blender - a 3d modeling and rendering package, 2025. 2

[9] Steve Cowen, Susan Briest, and James Dombrowski. Under- water docking of autonomous undersea vehicles using opti- cal terminal guidance. In *Proceedings of OCEANS*, pages 1143–1147. IEEE, 1997. 1

[10] Alexey Dosovitskiy, German Ros, Felipe Codevilla, Antonio Lopez, and Vladlen Koltun. Carla: An open urban driving simulator. In *Proceedings of the Conference on Robot Learn- ing*, pages 1–16, 2017. 3

[11] Junfeng Fan, Xiaoyan Liu, Yaming Ou, Pengju Zhang, Chao Zhou, and Zengguang Hou. Underwater robot self- localization method using tightly coupled events, images, in- ertial, and acoustic fusion. *IEEE Transactions on Industrial Electronics*, 72(5):5126–5135, 2025. 1

[12] Alessio Ferone, Marco Lazzaro, Vincenzo Mariano Scar- rica, Angelo Ciaramella, and Antonino Staiano. A synthetic dataset for learning optical flow in underwater environment. In *Applications of Artificial Intelligence and Neural Systems to Data Science*, pages 147–156. Springer, 2023. 2

[13] Epic Games. Unreal engine, 2025. 2

[14] Daniel Gehrig, Mathias Gehrig, Javier Hidalgo-Carrió, and Davide Scaramuzza. Video to events: Bringing modern com- puter vision closer to event cameras. *ArXiv*, abs/1912.03095, 2019. 3

[15] Mathias Gehrig, Willem Aarents, Daniel Gehrig, and Davide Scaramuzza. Dsec: A stereo event camera dataset for driv- ing scenarios. *IEEE Robotics and Automation Letters*, 6(3): 4947–4954, 2021. 6

[16] Mathias Gehrig, Mario Millhäuser, Daniel Gehrig, and Da- vide Scaramuzza. E-raft: Dense optical flow from event cam- eras. In *Proceedings of the International Conference on 3D Vision*, pages 197–206. IEEE, 2021. 6, 8

[17] Michele Grimaldi, Patryk Cieślak, Eduardo Ochoa, Vib- hav Bharti, Hayat Rajani, Ignacio Carlucho, Maria Koskinopoulou, Yvan R Petillot, and Nuno Gracias. Stone- fish: Supporting machine learning research in marine robotics. In *Proceedings of the IEEE International Conference on Robotics and Automation*, pages 1–7, 2025. 2

[18] Fengyue Guo, Peng Ren, and Cai Luo. Utnet: Event-rgb multi-modal fusion model for underwater transparent organ- ism detection. *Intelligent Marine Technology and Systems*, 3 (1):18, 2025. 2

[19] Friedhelm Hamann, Ziyun Wang, Ioannis Asmanis, Kenneth Chaney, Guillermo Gallego, and Kostas Daniilidis. Motion- prior contrast maximization for dense continuous-time motion estimation. In *Proceedings of the European Conference on Computer Vision*, pages 18–37. Springer, 2024. 6, 7, 8

[20] Kaiming He, Xiangyu Zhang, Shaoqing Ren, and Jian Sun. Deep residual learning for image recognition. In *Proceed- ings of the IEEE/CVF Conference on Computer Vision and Pattern Recognition*, pages 770–778, 2016. 2

[21] Yuhuang Hu, Shih-Chii Liu, and Tobi Delbruck. v2e: From video frames to realistic dvs events. In *Proceedings of the IEEE/CVF Conference on Computer Vision and Pattern Recognition*, pages 1312–1321, 2021. 3

[22] Md Jahidul Islam, Alberto Quattrini Li, Yogesh A Girdhar, and Ioannis Rekleitis. Computer vision applications in un- derwater robotics and oceanography. In *Computer Vision*, pages 173–204. Chapman and Hall/CRC, 2024. 1

[23] Reina Kaneko, Takumi Ueda, Hiroshi Higashi, and Yuichi Tanaka. Phiswid: Physics-inspired underwater image dataset synthesized from rgb-d images. *arXiv preprint arXiv:2404.03998*, 2024. 2, 3

[24] Pritam P Karmokar and William J Beksi. Inertia-informed orientation priors for event-based optical flow estimation. *arXiv preprint arXiv:2511.12961*, 2025. 6, 8

[25] Pritam P Karmokar, Quan H Nguyen, and William J Beksi. Secrets of edge-informed contrast maximization for event- based vision. In *Proceedings of the Winter Conference on Applications of Computer Vision*, pages 630–639, 2025. 6, 8

[26] Nathan Koenig and Andrew Howard. Design and use paradigms for gazebo, an open-source multi-robot simulator. In *Proceedings of the IEEE/RSJ International Conference on Intelligent Robots and Systems*, pages 2149–2154, 2004. 2

[27] Hitesh Kyatham, Arjun Suresh, Aadi Palnitkar, and Yiannis Aloimonos. Erebus: End-to-end robust event based under- water simulation. In *Proceedings of the IEEE International Conference on Robotics and Automation AQUA2SIM Work- shop*, 2025. 3, 6

[28] Shuangquan Li, Zhichen Zhang, Qixian Zhang, Haiyang Yao, Xudong Li, Jianjun Mi, and Haiyan Wang. Breakthrough underwater physical environment limitations on optical information representations: An overview and suggestions. *Journal of Marine Science and Engineering*, 12(7):1055, 2024. [1](#), [3](#)

[29] Songyang Li, Tingyu Liu, Qunyan Jiang, Yuanqi Li, Jie Guo, Lei Jiao, Yanwen Guo, and Zhonghua Ni. Realistic simulation of underwater scene for image enhancement. *IEEE Transactions on Geoscience and Remote Sensing*, 63:1–14, 2025. [3](#)

[30] Yijin Li, Zhaoyang Huang, Shuo Chen, Xiaoyu Shi, Hongsheng Li, Hujun Bao, Zhaopeng Cui, and Guofeng Zhang. Blinkflow: A dataset to push the limits of event-based optical flow estimation. In *Proceedings of the IEEE/RSJ International Conference on Intelligent Robots and Systems*, pages 3881–3888, 2023. [3](#)

[31] Yupeng Liao, Mingjia Shangguan, Zifeng Yang, Zaifa Lin, Yuanlun Wang, and Sihui Li. Gpu-accelerated monte carlo simulation for a single-photon underwater lidar. *Remote Sensing*, 15(21):5245, 2023. [2](#)

[32] Pål Liljebäck and Richard Mills. Eelume: A flexible and subsea resident imr vehicle. In *Proceedings of OCEANS*, pages 1–4. IEEE, 2017. [1](#)

[33] Xiaomin Lin, Nitesh Jha, Mayank Joshi, Nare Karapetyan, Yiannis Aloimonos, and Miao Yu. Oystersim: Underwater simulation for enhancing oyster reef monitoring. In *Proceedings of OCEANS*, pages 1–6. IEEE, 2022. [2](#)

[34] Shuang Liu, Mete Ozay, Takayuki Okatani, Hongli Xu, Kai Sun, and Yang Lin. Detection and pose estimation for short-range vision-based underwater docking. *IEEE Access*, 7:2720–2749, 2018. [1](#)

[35] Cai Luo, Jihua Wu, Shixin Sun, and Peng Ren. Transcodnet: Underwater transparently camouflaged object detection via rgb and event frames collaboration. *IEEE Robotics and Automation Letters*, 9(2):1444–1451, 2023. [2](#), [6](#)

[36] Xinglong Luo, Kunming Luo, Ao Luo, Zhengning Wang, Ping Tan, and Shuaicheng Liu. Learning optical flow from event camera with rendered dataset. In *Proceedings of the IEEE/CVF International Conference on Computer Vision*, pages 9847–9857, 2023. [3](#)

[37] Sadiq Layi Macaulay, Nimet Kaygusuz, and Simon Hadfield. Evtslowtv - a large and diverse dataset for event-based depth estimation. *arXiv preprint arXiv:2511.02953*, 2025. [2](#), [6](#)

[38] Rajini Makam, Dhatri Shankari T M, Sharanya Patil, and Suresh Sundram. Oceanlens: An adaptive backscatter and edge correction using deep learning model for enhanced underwater imaging. *arXiv preprint arXiv:2411.13230*, 2024. [3](#)

[39] Musa Morena Marcusso Manhães, Sebastian A Scherer, Martin Voss, Luiz Ricardo Douat, and Thomas Rauschenbach. Uuv simulator: A gazebo-based package for underwater intervention and multi-robot simulation. In *Proceedings of OCEANS*, pages 1–8. IEEE, 2016. [2](#)

[40] Jad Mansour, Hayat Rajani, Rafael Garcia, and Nuno Gracias. ecarla-scenes: A synthetically generated dataset for event-based optical flow prediction. *arXiv preprint arXiv:2412.09209*, 2024. [3](#)

[41] Jad Mansour, Sebastian Realpe, Hayat Rajani, Michele Grimaldi, Rafael Garcia, and Nuno Gracias. estonefish-scenes: A synthetically generated dataset for underwater event-based optical flow prediction tasks. *arXiv preprint arXiv:2505.13309*, 2025. [3](#), [6](#)

[42] Ahmed Mohammed, Johannes Kvam, Jens T Thielemann, Karl H Haugholt, and Petter Risholm. 6d pose estimation for subsea intervention in turbid waters. *Electronics*, 10(19):2369, 2021. [1](#)

[43] Shahriar Negahdaripour and Pezhman Firoozfam. An rov stereovision system for ship-hull inspection. *IEEE Journal of Oceanic Engineering*, 31(3):551–564, 2007. [1](#)

[44] Mikkel Cornelius Nielsen, Mari Hovem Leonhardsen, and Ingrid Schjølberg. Evaluation of posenet for 6-dof underwater pose estimation. In *Proceedings of OCEANS*, pages 1–6. IEEE, 2019. [1](#)

[45] Alvaro Novo, Francisco Lobon, Hector Garcia de Marina, Samuel Romero, and Francisco Barranco. Neuromorphic perception and navigation for mobile robots: A review. *ACM Computing Surveys*, 56(10), 2024. [1](#)

[46] Yifan Peng, Yuze Hong, Ziyang Hong, Apple Pui-Yi Chui, and Junfeng Wu. Aquaticvision: Benchmarking visual slam in underwater environment with events and frames. *arXiv preprint arXiv:2505.03448*, 2025. [1](#), [2](#), [6](#)

[47] Yelena Randall and Tali Treibitz. Flsea: Underwater visual-inertial and stereo-vision forward-looking datasets. *arXiv preprint arXiv:2302.12772*, 2023. [2](#)

[48] Henri Rebecq, Daniel Gehrig, and Davide Scaramuzza. Esim: An open event camera simulator. In *Proceedings of the Conference on Robot Learning*, pages 969–982. PMLR, 2018. [3](#)

[49] Ivar Bjørgo Saksvik, Håkon Weydahl, Håkon Teigland, Alex Alcocer, and Vahid Hassani. Towards an open-source benchmark for underwater object detection and pose estimation. In *Proceedings of the IEEE Conference on Underwater Technology*, pages 1–5, 2023. [1](#), [6](#)

[50] Patricia Schöntag, David Nakath, Judith Fischer, Rüdiger Röttgers, and Kevin Köser. Optical ocean recipes: Creating realistic datasets to facilitate underwater vision research. *arXiv preprint arXiv:2509.20171*, 2025. [3](#)

[51] Anne Sedlazeck and Reinhard Koch. Simulating deep sea underwater images using physical models for light attenuation, scattering, and refraction. In *Proceedings of Vision, Modeling, and Visualization*. The Eurographics Association, 2011. [3](#)

[52] Shital Shah, Debadeepa Dey, Chris Lovett, and Ashish Kapoor. Airsim: High-fidelity visual and physical simulation for autonomous vehicles. In *Proceedings of the International Conference on Field and Service Robotics*, pages 621–635. Springer, 2017. [2](#)

[53] Chandan Sheikder, Weimin Zhang, Xiaopeng Chen, Fangxing Li, Yichang Liu, Zhengqing Zuo, Xiaohai He, and Xinyan Tan. Marine-inspired multimodal sensor fusion and neuromorphic processing for autonomous navigation in unstructured subaqueous environments. *Sensors*, 25(21):6627, 2025. [1](#)

[54] Shintaro Shiba, Yoshimitsu Aoki, and Guillermo Gallego. Secrets of event-based optical flow. In *Proceedings of the*

European Conference on Computer Vision, pages 628–645. Springer, 2022. [6](#), [7](#), [8](#)

- [55] Aaron Steiner. Understanding the basics of underwater lighting. *Ocean News & Technology*, 19(4):10–12, 2013. [1](#)
- [56] Håkon Teigland, Vahid Hassani, and Ments Tore Møller. Operator focused automation of rov operations. In *Proceedings of the IEEE/OES Autonomous Underwater Vehicles Symposium*, pages 1–7, 2020. [1](#)
- [57] Xiaotian Wang, Xinnan Fan, Yueyue Liu, Yuanxue Xin, and Pengfei Shi. Eum-slam: An enhancing underwater monocular visual slam with deep learning-based optical flow estimation. *IEEE Transactions on Instrumentation and Measurement*, 2025. [1](#)
- [58] Daniel Yang, John J Leonard, and Yogesh Girdhar. Seasplat: Representing underwater scenes with 3d gaussian splatting and a physically grounded image formation model. In *Proceedings of the IEEE International Conference on Robotics and Automation*, pages 7632–7638, 2025. [3](#)
- [59] Amir Mehdi Yazdani, Karl Sammut, Oleg Yakimenko, and Andrew Lammes. A survey of underwater docking guidance systems. *Robotics and Autonomous Systems*, 124:103382, 2020. [1](#)
- [60] Peng Yue, XiangRu Wang, Shan Xu, and YunLong Li. Monte-carlo based non-line-of-sight underwater wireless optical communication channel modeling and system performance analysis under turbulence. *arXiv preprint arXiv:2501.12859*, 2025. [2](#)
- [61] Mabel M Zhang, Woen-Sug Choi, Jessica Herman, Duane Davis, Carson Vogt, Michael McCarrin, Yadunund Vijay, Dharini Dutia, William Lew, Steven Peters, and Brian Bingham. Dave aquatic virtual environment: Toward a general underwater robotics simulator. In *Proceedings of the IEEE/OES Autonomous Underwater Vehicles Symposium*, pages 1–8, 2022. [1](#)
- [62] Peder Georg Olofsson Zwigmeyer, Mauhing Yip, Andreas Langeland Teigen, Rudolf Mester, and Annette Stahl. The varos synthetic underwater data set: Towards realistic multi-sensor underwater data with ground truth. In *Proceedings of the IEEE/CVF International Conference on Computer Vision*, pages 3722–3730, 2021. [2](#), [3](#)